NASA TM X-447

TECHNICAL MEMORANDUM

X-447

TRANSONIC FLUTTER INVESTIGATION OF MODELS OF THE X-15 AIRPLANE HORIZONTAL TAIL

By Lou S. Young and Samuel R. Bland

Langley Research Center
Langley Field, Va.

NATIONAL AERON[illegible] AND SPACE ADMINISTRATION
WASHINGTON

February 1961

NATIONAL AERONAUTICS AND SPACE ADMINISTRATION

TECHNICAL MEMORANDUM X-447

TRANSONIC FLUTTER INVESTIGATION OF MODELS OF THE X-15 AIRPLANE HORIZONTAL TAIL*

By Lou S. Young and Samuel R. Bland

SUMMARY

A flutter investigation of models of the sweptback, tapered, all-movable horizontal tail of the X-15 airplane was made in the Langley transonic blowdown tunnel at Mach numbers between 0.72 and 1.32. The models were dynamically and elastically scaled so that the elastic scaling included a flutter safety margin. Therefore, in order for the models to indicate an adequate safety margin for the airplane, they were required to be flutter free at dynamic pressures up to the simulated maximum dynamic pressure for the airplane. The stiffness distributions of the airplane tail panels to which the elastic scaling was applied were those calculated for a reduced skin stiffness resulting from transient aerodynamic heating. This condition occurred at a very high Mach number and altitude. During descent, as the Mach number approaches transonic values, the stiffnesses would tend to increase; therefore, the results obtained for the present models may be conservative.

Full-span models were used in the investigation, and the panels were independently mounted to simulate the airplane tail panels. Some semispan models were also tested. The panels were attached to a mass which was flexibly mounted in a sting fuselage so that the models had solid-body freedoms in pitch, roll, and vertical translation.

The results indicated that the airplane horizontal tail has the required flutter safety margin at transonic speeds.

author

INTRODUCTION

The Langley Research Center has undertaken a program of flutter testing components of the X-15 airplane over a range of speeds. Included in this program have been investigations of models of three

*Title, Unclassified.

different designs for the all-movable horizontal tail. The three designs differed somewhat in the distributions of mass and stiffness. The original design has been investigated at transonic, supersonic, and hypersonic speeds (refs. 1, 2, and 3, respectively). A revised design for the tail was also investigated at transonic speeds in reference 1. The final design (used on the airplane) has been the subject of a hypersonic investigation (ref. 4) and is the subject of the present investigation, which was made at Mach numbers between 0.72 and 1.32 in the Langley transonic blowdown tunnel. The models used in the investigation were dynamically and elastically scaled from the properties of the final design for the tail. The stiffness distributions of the airplane tail panels to which the elastic scaling was applied were those calculated for a reduced skin stiffness resulting from transient aerodynamic heating. (See ref. 5.) The transient heating effects were calculated for that part of the flight path which gave the greatest stiffness reduction. This condition occurred at a very high Mach number and altitude. During descent, as the Mach number approaches transonic values, the stiffnesses would tend to increase; therefore, the results obtained for the present models may be conservative.

L 1 0 1 6

Full-span models were used in the investigation, and the panels were independently mounted to simulate the airplane tail panels. The pitching stiffness for the models was varied from approximately 104 percent to 163 percent of the scaled airplane value. The tail panels were attached to a mass which was flexibly mounted in a sting fuselage so that the model had solid-body freedoms in pitch, roll, and vertical translation. Some of the panels were tested singly after their companion panels had been destroyed.

SYMBOLS

a	speed of sound, ft/sec
b_a	average streamwise semichord of exposed panel, ft
b_r	root semichord of exposed panel, ft
b_t	tip semichord of panel, ft
EI	bending stiffness, lb-ft^2
f_f	flutter frequency, cps
f_i	frequency of ith natural vibration mode (i = 1,2,3, . . . 16), cps
g	structural damping coefficient of first natural vibration mode

[redacted]

GJ torsional stiffness, lb-ft^2

I_θ moment of inertia of panel (including spindle) in pitch about pitch axis, slug-ft^2

k_θ simulated panel pitching stiffness at intersection of panel root and pitch axis with respect to simulated fuselage mass, ft-lb/radian

L 1016

l length scale factor, $\frac{\text{Typical model length}}{\text{Corresponding airplane length}}$

M Mach number

m mass scale factor, $\frac{\text{Typical model mass}}{\text{Corresponding airplane mass}}$

m' mass of panel (including spindle), slugs

q dynamic pressure, $\frac{1}{2}\rho V^2$, lb/sq ft

s span of panel, ft

T static temperature, $^\circ R$

t time scale factor,

$$\frac{\text{Time for tunnel airstream to move 1 model tail chord}}{\text{Time for airplane to move 1 airplane tail chord}}$$

V velocity, ft/sec

$\bar{V}$ reduced velocity based on a representative natural vibration frequency, $V/b_a 2\pi f_i$

v volume of frustum of cone enclosing the tail panel, $\pi\frac{s}{3}\left(b_r^2 + b_r b_t + b_t^2\right)$, cu ft

ζ natural-vibration-frequency reduction factor used to provide a margin of safety in application of model flutter test results to airplane

η nondimensional distance along reference axis,

$$\frac{\text{Distance from panel root along reference axis}}{\text{Length of exposed panel reference axis}}$$

[redacted]

μ	mass ratio, $m'/\rho v$
ρ	static air density, slugs/cu ft
ω_f	circular flutter frequency, radians/sec
ω_α	frequency of predominantly torsional natural vibration mode, $2\pi f_\beta$ for the models, radians/sec

Subscripts:

A	airplane
a	actual
M	model
t	truly scaled

MODELS

Configurations

The four models used in the investigation are designated by the numbers 1, 2, 3, or 4. Each of the separate tail panels is designated by the number of the model in which it was used, and the letter L or R follows each number to indicate whether it was a left or right panel, respectively. The models are generally treated herein in terms of the separate panels because some of the panels were tested singly after their companion panels had been destroyed. Models 3 and 4 had close to the scaled value of pitching stiffness, while models 1 and 2 had values of pitching stiffness which were considerably higher.

Geometry

The full-span models were 1/12-size versions of the horizontal tail panels of the airplane. A sketch of a typical model giving basic dimensions is shown in figure 1.

The models had a planform incorporating about 45° sweepback of the quarter-chord line, an exposed panel aspect ratio of 1.258, and an exposed panel taper ratio of 0.299. The streamwise airfoil section derived by the manufacturer was a 66A005, which was modified to have a 1-percent-chord thickness at the trailing edge, with a straight-line fairing from

the trailing edge to the 67-percent-chord point (point of tangency). Near the tip, the airfoil was modified further by increasing the thickness ahead of the 15-percent-chord line. Airfoil ordinates are presented in figure 1, and some model geometric properties are listed in table I. A photograph of a model mounted in the sting and a cross-section sketch of the sting are shown in figure 2.

Scaling

Scaling the airplane properties required that the nondimensional mass and stiffness distributions be the same for the model and the airplane. The mass and stiffness levels for the model were obtained by specifying the scale factors for the fundamental quantities involved; that is, length, mass, and time.

The size of the models was limited by tunnel-wall interference considerations. On the basis of previous experience, the length scale factor was chosen to be

$$l = \frac{1}{12} \tag{1}$$

The mass scale factor was obtained from the requirement that the mass ratio μ be the same for both model and airplane and is as follows:

$$m = \frac{\rho_M}{\rho_A} l^3 \tag{2}$$

The density ratio was chosen to be $\frac{\rho_M}{\rho_A} = 1.275$.

The time scale factor was derived from the requirement that the reduced velocity $\overline{V}$ be the same for the model as for the airplane and is as follows:

$$t = \left(\frac{V_M}{V_A}\right)^{-1} l$$

Since the Mach number is the same for both model and airplane,

[redacted]

$$t = \left(\frac{T_M}{T_A}\right)^{-1/2} l \qquad (3)$$

The static temperature for the airplane T_A is a function only of altitude, and for sea-level altitude T_A was taken to be 519° R. However, during a tunnel run, the temperature drops continually as air is expended from the reservoir. A study of flutter data obtained during earlier investigations indicated that 408° R was near the average value of T_M that could be expected during the present tests. These values of T_M and T_A were used in equation (3); hence, 0.786 was used as the value of T_M/T_A.

The pertinent model and flow quantities and the design scale factors which apply to them are listed in table II. The scaling approach for these models differed from that used for the X-15 horizontal tail models described in reference 1 by the use of the factor ζ which appears in the scale factors for some of the quantities listed in table II. The factor ζ, which has the value of 0.85, reduces the natural vibration frequencies to 85 percent of those which would result from application of the scale factors as specified (eqs. (1), (2), and (3)). The frequency reduction was accomplished by reducing the stiffnesses the appropriate amount; thus, the values of EI, GJ, and k_θ in table II are multiplied by the factor ζ^2. The purpose of reducing the model frequencies was to provide a margin of safety in the application of the model flutter test results to the airplane. The designed reduced velocity for the model is thus equal, not to that of the airplane, but to that of an airplane having stiffnesses 72.25 percent ($\zeta^2 = 0.85^2$) of those calculated for the actual airplane for a reduced skin stiffness resulting from transient aerodynamic heating.

The dynamic pressure and Mach number are quantities which are controllable during a run; whereas, the temperature is not controllable. When the dynamic pressure and Mach number are considered to be fixed and a static temperature different from the design value is obtained, both the density and velocity will be different from the values considered in the scaling. The density and velocity changes result in values of mass ratio and reduced velocity, respectively, different from the design values. However, a combination of reduced velocity and mass ratio, which can be expressed in terms of the dynamic pressure $\frac{\bar{V}_M^2}{\mu_M} \propto q_M$, is independent of the temperature. On the basis of this parameter, a truly scaled model would exactly simulate the airplane in the tests because the simulated altitude is interpreted in terms of the dynamic pressure. Thus, the scale factor for dynamic pressure in table II is used to convert the dynamic pressure for the airplane at any Mach number and altitude to the dynamic pressure for the model at the same Mach number and altitude.

The dynamic pressure for the airplane is assumed to be that of the ICAO standard atmosphere (ref. 6). For a given altitude, q/M^2 has a constant value.

The effect of not individually satisfying exactly the mass-ratio and reduced-velocity requirements is believed to be negligible in the present investigation. Experience with a wide variety of flutter models has indicated that, at a given Mach number, flutter tends to occur at a constant value of dynamic pressure regardless of the individual values of density and velocity, at least within the operational limits of the tunnel.

Construction

The panel construction is shown in figure 3, which is an X-ray photograph of panel 4R. Each panel had a balsa-filled aluminum box spar to which the aluminum ribs were fastened. The magnesium spindle (fig. 1) was integral with the root rib, which fitted into the spar root. Panels 4L and 4R had slightly different construction from the other panels as indicated in figure 3. The structure described thus far was held together by means of a resinous glue reinforced with small aluminum nails which can be seen in figure 3. The rest of the structure, consisting of pine leading and trailing edges and balsa wood to fill out the airfoil shape, was glued to the spar and ribs. Lead weights were also glued into the structure at various points to obtain the desired mass distribution.

Each panel was fastened to the fuselage mass by means of two pairs of flexure pivots which fixed the pitch axis (fig. 4). The pitching-stiffness level was controlled by a bronze spring cantilevered from the spindle (fig. 4), which was connected to the fuselage mass by means of a long screw. The fuselage mass was made of steel and lead pieces, which were supported forward and rearward by springs cantilevered from the sting mounting block. A schematic sketch showing the arrangement of the fuselage mass is given in figure 4, and figure 5 shows a photograph of a model in the sting mounting block which is removed from the sting and the wooden fairing blocks.

Physical Properties

Natural vibration modes.- The frequencies and node lines of the natural vibration modes were found for each model just prior to flutter testing. The models were excited by means of an electromagnetic shaker fitted with a double-pronged stem so that both panels could be excited simultaneously. Node lines were located during the resonant vibrations by sprinkling sand on the model. The results of these measurements are given in figure 6 and in table III. A description of each of the natural vibration modes is given in table III(a), and the frequencies found on

each panel are listed in table III(b). It may be noted in table III(b) that modes in addition to those found on the airplane were found on the models. Of the panels which were tested singly after the destruction of their companion panels, only 4R was vibrated before flutter testing without another panel in the mount. The modal characteristics of the predominantly first and second symmetrical bending and first symmetrical torsional modes were essentially the same for 4R alone as for 4R when it was vibrated in the complete model 4.

The averaged values of the structural damping coefficient in the first natural vibration mode, as determined for each panel from records of the decay of oscillations induced by plucking the panel in still air, are presented in table III(b).

Stiffness measurements.- The pitching stiffness at the intersection of the pitch axis with the panel root (fig. 1) was measured for each panel by means of an optical system employing a cathetometer. These values of k_θ are listed in table III(b).

The bending and torsional stiffness distributions were measured for panels 1R and 4L by means of an optical system which is described in reference 7. These panel stiffness distributions are plotted in figure 7 along with the scaled airplane stiffness distributions (ref. 8). The reference axis used for the stiffness distribution measurements was the 53-percent-chord line.

A value of approximately 20,000 ft-lb/radian was obtained for the pitching stiffness of the fuselage mass at the panel pitch axis (fig. 4). The mode shape of the fuselage mass for the pitching mode was not determined; thus, the degree of simulation of the generalized fuselage mass for this mode is not known. Measurements of the stiffnesses in roll and vertical translation were not made.

Mass properties.- The mass and center-of-gravity location of each panel (including the spindle) are presented in table III(b). The panel mass distributions were not measured for these models; this property was scaled from the airplane (ref. 8).

The moment of inertia of each panel and spindle in pitch about the pitch axis is also given in table III(b). The moment-of-inertia data for all of the panels except 4L and 4R were supplied by the model manufacturer; the values of moment of inertia for panels 4L and 4R were measured by means of a bifilar pendulum and were obtained by transferring the moment of inertia about the center of gravity, with the assumption that the center of gravity was located in the model horizontal plane.

The spindles of several of the models, which were broken during flutter testing, were cut off at the panel root and their average mass

was found to be 0.596×10^{-3} slug with a center-of-gravity location 0.073 foot from the panel root. The fuselage mass without the panels but including one-half the mass of the forward and rearward springs was 0.235 slug with a center-of-gravity location 0.046 foot forward of the panel pitch axis.

APPARATUS AND TESTS

The flutter tests were made in the Langley transonic blowdown tunnel which has a slotted test section. The test section is octagonal in cross section and measures $26\frac{1}{4}$ inches between sides. During operation of the tunnel, a preselected Mach number is set by means of a variable orifice downstream of the test section. This Mach number is held approximately constant after the orifice is choked while the stagnation pressure and, thus, the density are increased. However, the runs of the present investigation were generally made at dynamic pressures which were too low to choke the orifice so that Mach number and density both increased during the runs. The static-density range is approximately 0.001 to 0.012 slug per cubic foot, and Mach numbers may be obtained from subsonic values to a maximum of about 1.4. It should be noted that, because of the expansion of the air in the reservoir during a run, the stagnation temperature continually decreases; thus, the test-section velocity is not uniquely defined by the Mach number. Additional information about the tunnel is contained in reference 9. Excellent agreement between flutter data obtained in the tunnel and data obtained in free air has been observed (ref. 10).

In the present flutter tests, the models were mounted in a sting as shown in figure 2. The sting extended upstream into the subsonic flow region of the tunnel to prevent the formation of shock waves off the fuselage nose, which might be reflected back onto the model. The sting and model weighed approximately 305 pounds, and the system had a fundamental bending frequency of about 15 cycles per second. The two panels were carefully alined to be at zero angle of attack in the tunnel, and tunnel runs to check this trim were made. Wire strain gages were mounted on each panel spar, as sketched in figure 1, and were oriented so as to indicate panel deflections about predominantly bending and torsional axes. The strain-gage signals, the tunnel stagnation and static pressures, and the stagnation temperature were recorded by a recording oscillograph. The strain-gage traces on the oscillograph records were used to identify the start of flutter and to obtain the flutter frequency. High-speed motion pictures were made during some of the runs and were used in observing the flutter mode. Two cameras were used; one camera photographed only the left panel of each model, and the other camera photographed the lower surfaces of both panels. The cameras were used either simultaneously or in sequence during the runs.

The tests were made at Mach numbers between 0.72 and 1.32 and at simulated altitudes down to below sea level.

RESULTS AND DISCUSSION

Interpretation of Results

As stated in the section entitled "Scaling," the model stiffnesses, with the exceptions of k_θ for models 1 and 2, were 72.25 percent of the values which would be obtained from scaling the airplane stiffnesses without the use of the factor ζ^2. Thus, the simulated altitudes for the model are to be interpreted as altitudes which, if cleared by the model, could be reached with a 38.4-percent margin of safety in stiffness $\left(\frac{1}{0.7225} = 1.384\right)$ by the airplane, if the model is assumed to closely simulate the airplane in all respects. The results may be interpreted alternatively by considering that a flutter point obtained with the model represents an airplane flutter point at the same Mach number at a simulated altitude corresponding to a dynamic pressure 38.4 percent higher than that for the model.

The criterion for determining whether the closely scaled models (models 3 and 4) indicated that the airplane would have an adequate flutter safety margin was that the models should be flutter free up to the simulated maximum dynamic pressure for the airplane at the various Mach numbers. As discussed in the introduction, the model results may be conservative because the models were scaled from airplane properties which were calculated for a transient aerodynamic heating condition which was probably more severe than would be encountered at transonic Mach numbers.

The oscillograph records of several of the test runs showed a period of intermittent sinusoidal oscillations of the model prior to the advent of the steady sinusoidal oscillations of increasing amplitude which indicated flutter. In those cases where these intermittent oscillations tended to obscure the actual start of flutter, these regions have been defined as low-damping regions, and data at the start of such oscillations are included in the figures and tables. It is not known what significance the low-damping regions have for the airplane, since such oscillations may be in part a function of tunnel turbulence, which is different from turbulence in the atmosphere.

Discussion of Results

The data obtained in the 15 runs of this investigation are summarized in table IV, where the data points for each panel are presented in time

sequence for each run. The data given in table IV for the closely scaled models (models 3 and 4) are plotted in figure 8 in the form of dynamic pressure versus Mach number. Also shown in figure 8 are lines representing simulated sea-level and 10,000-foot altitudes, and the maximum airplane dynamic pressure. Since models 3 and 4 have values of pitching stiffness which were close to the scaled value (table III(b)), the results indicate that the airplane would have the required flutter safety margin.

The dynamic-pressure data for models 1 and 2 (table IV) are plotted in figure 9 as a function of Mach number. The same lines as in figure 8, representing simulated sea-level altitude, 10,000-foot altitude, and the maximum airplane dynamic pressure, are shown in figure 9. As may be seen in table III(b), the pitching-stiffness values for these models averaged about 157 percent of the scaled values and, as would be expected, greater flutter safety margins are indicated for the higher pitching stiffness than for the lower pitching stiffness. (Compare figs. 8 and 9.)

High-speed motion pictures were taken during all of the runs, but sequences during flutter were obtained only for panels 1L, 1R, 2L, and 4L. All of the motion pictures showed random yawing and pitching oscillations during most of each run, prior to flutter. The flutter mode was of the bending-torsion type wherein the torsion blended into quite large pitching deflections at the root. The flutter oscillations diverged rapidly until the panel broke.

The fuselage motions were imperceptible except during the most violent flutter oscillations, when some very slight motion was noted. The motion pictures of run 8 on model 1 show that, although at the start of each burst of low damping the panel motions were in phase, at the start of flutter the panels appeared to be completely independent.

In an attempt to correlate the data obtained on the models with the two levels of pitching stiffness (figs. 8 and 9), the following relation was assumed:

$$\left(\frac{b_a q}{m'\omega_\alpha^2}\right)_{M,t} = \left(\frac{b_a q}{m'\omega_\alpha^2}\right)_{M,a} \tag{4}$$

The quantities within the parentheses are nondimensional. The subscript M,t denotes the truly scaled model, and the subscript M,a denotes the actual model. The parameter $\frac{b_a q}{m'\omega_\alpha^2}$ is related to two other frequently

[redacted]

used parameters $\frac{V}{b_a\omega_\alpha\sqrt{\mu}}$ and $\frac{b_a\omega_\alpha\sqrt{\mu}}{a}$ as follows:

$$\frac{b_a q}{m'\omega_\alpha^2} = \left(\frac{V}{b_a\omega_\alpha\sqrt{\mu}}\right)^2\left(\frac{b_a^3}{2v}\right) = \frac{1}{\left(\frac{b_a\omega_\alpha\sqrt{\mu}}{a}\right)^2}\left(\frac{M^2 b_a^3}{2v}\right)$$

The relation in equation (4) is only approximate and is based on two assumptions. The first assumption is that flutter at a given Mach number occurs at a given value of dynamic pressure regardless of the individual values of density and velocity (as discussed under "Scaling"). The second assumption is that the dynamic pressure for flutter varies directly with the model mass and directly with the square of the torsion frequency. Thus, the relation cannot take any account of a difference in mass distribution between the truly scaled and the actual model. The difference in pitching stiffness between the truly scaled and the actual model is accounted for only on the basis of the effect of pitching stiffness on the torsion frequency. The dynamic pressure for flutter for a truly scaled model is desired and may be obtained from equation (4) by transposing; thus,

$$q_{M,t} = \left(\frac{m'_{M,t}}{m'_{M,a}}\right)\left(\frac{\omega_{\alpha_{M,t}}}{\omega_{\alpha_{M,a}}}\right)^2 q_{M,a} \qquad (5)$$

where the semichords have been dropped because they are equal.

The data of figures 8 and 9, corrected on the basis of equation (5) to true model mass and torsion frequency values, are shown in figure 10. The data correlate over a band which lies at dynamic pressures higher than the scaled maximum dynamic pressures of the airplane and, thus, indicate at least the required 38.4-percent margin of flutter safety in stiffness.

CONCLUSION

A transonic flutter investigation was made of models of the all-movable horizontal tail of th[redacted]lane. The stiffnesses of the

[redacted]

models were scaled from airplane properties which were calculated for a transient aerodynamic heating condition. This condition occurred at a very high Mach number and altitude. The resulting model stiffnesses were reduced more severely than the airplane stiffnesses would be at transonic Mach numbers during a normal descent; therefore, the model results may be conservative. The results indicate that the airplane horizontal tail has the required flutter safety margin at transonic speeds.

L
1
0
1
6

Langley Research Center,
National Aeronautics and Space Administration,
Langley Field, Va., October 31, 1960.

[redacted]

REFERENCES

1. Young, Lou S.: Transonic Flutter Investigation of Models of Proposed Horizontal Tails for the X-15 Airplane. NASA TM X-442, 1961.

2. Lauten, William T., Jr., and Hess, Robert W.: Experimental and Calculated Supersonic Flutter Characteristics of Models of the X-15 Horizontal and Vertical Tails. NASA TM X-176, 1959.

3. Lauten, William T., Jr., Levey, Gilbert M., and Armstrong, William O.: Investigation of an All-Movable Control Surface at a Mach Number of 6.86 for Possible Flutter. NACA RM L58B27, 1958.

4. Gibson, Frederick W., and Mixon, John S.: Flutter Investigation at a Mach Number of 7.2 of Models of the Horizontal- and Vertical-Tail Surfaces of the X-15 Airplane. NASA MEMO 4-14-59L, 1959.

5. Landrum, L. L.: Estimated Aeroelastic Characteristics for the X-15 Airplane (NAA Model Designation NA-240). Rep. No. NA-59-471, North American Aviation, Inc., Apr. 16, 1959.

6. Anon.: Standard Atmosphere - Tables and Data for Altitudes to 65,800 Feet. NACA Rep. 1235, 1955. (Supersedes NACA TN 3182.)

7. Land, Norman S., and Abbott, Frank T., Jr.: Method of Controlling Stiffness Properties of a Solid-Construction Model Wing. NACA TN 3423, 1955.

8. Sweet, H. R.: A Specification for the Flutter Models of the X-15 Flutter Program. Rep. No. NA-56-738, North American Aviation, Inc., Aug. 17, 1956.

9. Unangst, John R., and Jones, George W., Jr.: Some Effects of Sweep and Aspect Ratio on the Transonic Flutter Characteristics of a Series of Thin Cantilever Wings Having a Taper Ratio of 0.6. NACA RM L55I13a, 1956.

10. Bursnall, William J.: Initial Flutter Tests in the Langley Transonic Blowdown Tunnel and Comparison With Free-Flight Flutter Results. NACA RM L52K14, 1953.

L 1 0 1 6

TABLE I.- GEOMETRIC PROPERTIES OF MODELS

Streamwise airfoil section	Modified 66A005
Sweepback of quarter-chord line, deg	44.6
Panel span, ft	0.476
Streamwise panel root chord, ft	0.583
Panel area, sq ft	0.180
Panel aspect ratio	1.258
Panel taper ratio	0.299
Planform semispan, ft	0.665
Maximum streamwise chord based on extension of panel to fuselage center line, ft	0.745
Planform area sq ft	0.611
Planform aspect ratio	2.893
Planform taper ratio	0.234

TABLE II.- DESIGN SCALE FACTORS OF PERTINENT

MODEL AND FLOW QUANTITIES

$$\left[\frac{\rho_M}{\rho_A} = 1.275;\ \frac{T_M}{T_A} = 0.786;\ \zeta = 0.85\right]$$

Quantity	Design scale factor	
	Symbolical	Numerical
Fundamental quantities		
Length	l	1/12
Mass	$m = \left(\frac{\rho_M}{\rho_A}\right) l^3$	7.378×10^{-4}
Time	$t = \left(\frac{T_M}{T_A}\right)^{-1/2} l$	9.400×10^{-2}
Derived quantities		
Stream velocity	lt^{-1}	0.8865
Stream dynamic pressure	$ml^{-1}t^{-2}$	1.002
Moment of inertia	l^2m	5.124×10^{-6}
k_θ	$\zeta^2 l^2 mt^{-2}$	4.189×10^{-4}
EI and GJ	$\zeta^2 l^3 mt^{-2}$	3.491×10^{-5}
Natural vibration frequency	ζt^{-1}	9.043

TABLE III.- PHYSICAL PROPERTIES OF MODELS

(a) Description of natural vibration modes

Mode number	Predominant characteristic	Symmetrical or antisymmetrical	Panel pitching motion	Coupling between panels	Fuselage motion	Remarks
1	First bending	Symmetrical when panels coupled	Some	Very little	None	Strong mode on each panel.
2	Fuselage translation or pitch	Symmetrical	None	(a)	Weak translation or pitch	Panel response weak.
3	Symmetrical yaw	[b]Symmetrical	------	Strong	----------	Weak mode; coupled with 5 on several models.
4	Antisymmetrical yaw	Antisymmetrical	------	Strong	----------	Stronger mode than 3; tended to be coupled with 14.
5	Antisymmetrical torsion	Antisymmetrical	Some	Strong	Rolled down on side where panel leading edge moved down	This mode was weak on model 2 which had a different frequency on each panel.
6	Antisymmetrical torsion	Antisymmetrical	Some	Weak	----------	Same as 5, but appeared only on panel 3R which also responded strongly in 5.
7	Coupled mode	[c]Symmetrical	Slight	Strong	----------	Apparently a coupling of 4, 8, and 14 which was strong when it appeared.
8	Symmetrical torsion	Symmetrical	Large	Strong	Some indefinite	Strong mode; panel torsion blended into pitch deflection.
9	Symmetrical torsion	Symmetrical	Large	Strong	Some indefinite	Same as 8, but appeared only on model 4; was apparently the natural torsion mode of panel 4L which also responded in mode 8.
10	Coupled torsion	----------	Some	------	----------	Appeared only on panel 4R alone in mount; this mode is probably same as 5, but included some yaw; tip went forward as it went up.
11	Symmetrical second bending	Symmetrical	Some	Strong	Very slight	Strong mode.
12	Antisymmetrical second bending	Antisymmetrical	Slight	Strong	Slight	Modes 11 and 12 sweep into one another.
13	Symmetrical bending	Symmetrical	------	Strong	----------	Weak mode; apparently a natural frequency of panel 3L only, but the mode was coupled with the whole model.
14	Antisymmetrical second torsion	Antisymmetrical	------	Strong	----------	Strong mode; appeared on most models, but was recorded only on model 4; coupled with modes 4 and 7 in some instances.
15	Symmetrical second torsion	Symmetrical	------	------	----------	Not recorded for most models; node line recorded for 4R alone only.
16	Symmetrical third bending	Symmetrical	------	Strong	----------	Node lines not recorded; frequencies recorded for 4L and 4R alone only.

[a]Gages indicated different panel frequencies for some models.

[b]Panel tips move in same direction.

[c]Had some yawing motion which was antisymmetrical.

TABLE III.- PHYSICAL PROPERTIES OF MODELS - Concluded

(b) Compiled physical properties

Model	Panel	Natural vibration frequencies, cps																Structural damping coefficient, g	Root pitching stiffness, k_θ, ft-lb/radian	Panel mass, m', slugs	Center-of-gravity location, ft		Moment of inertia of panel and spindle about pitch axis, I_θ, slug-ft^2
		f_1	f_2	f_3	f_4	f_5	f_6	f_7	f_8	f_9	f_{10}	f_{11}	f_{12}	f_{13}	f_{14}	f_{15}	f_{16}				Behind pitch axis	Out from panel root	
1	L	112	150	---	---	297	---	---	332	---	---	387	440	---	---	523	---	0.015	494	0.580×10^{-2}	0.077	0.156	[a] 1.630×10^{-4}
	R	110	150	---	---	297	---	---	327	---	---	387	440	---	---	---	---	0.017	508	0.590×10^{-2}	0.078	0.154	[a] 1.603×10^{-4}
2	L	112	146	232	---	264	---	---	340	---	---	390	429	---	---	---	---	0.022	492	0.591×10^{-2}	0.073	0.157	[a] 1.741×10^{-4}
	R	108	150	232	---	259	---	---	335	---	---	388	431	---	---	---	---	0.025	460	0.596×10^{-2}	0.074	0.158	[a] 1.683×10^{-4}
3	L	106	145	182	237	276	---	---	301	---	---	383	430	331	---	---	---	0.020	348	0.593×10^{-2}	0.078	0.160	[a] 1.679×10^{-4}
	R	102	140	182	237	276	283	---	302	---	---	383	430	331	---	---	---	0.022	334	0.589×10^{-2}	0.077	0.157	[a] 1.669×10^{-4}
4	L	108	149	179	234 to 240	278	---	234	300	264	---	383	333	---	480	520	840	0.021	327	0.634×10^{-2}	0.072	0.160	1.793×10^{-4}
	R	106	148	179	234 to 240	278	---	234	300	264	---	380	333	---	480	527	---	0.018	325	0.626×10^{-2}	0.072	0.158	1.788×10^{-4}
4R alone		106	---	---	---	---	---	---	300	---	216	376	---	---	---	505	765	0.018	325	0.626×10^{-2}	0.072	0.158	1.788×10^{-4}
Scaled values		115	143	---	---	---	---	---	305	---	---	408	---	---	---	559	---	-----	312	0.584×10^{-2}	0.067	0.140	1.728×10^{-4}

[a]Data supplied by model manufacturer.

TABLE IV.- COMPILATION OF TEST RESULTS

Model	Run	Panel behavior (a)		f_f, cps	M	q, lb/sq ft	V, ft/sec	ρ, slugs/cu ft	T, °R	μ		$\frac{b_a \omega_f}{V}$
		Left (L)	Right (R)							Left panel	Right panel	
1	1	Q	Q		0.724	1,342	747	0.0046	467	----	----	
	2	Q	Q		.882	1,568	919	.0037	452	----	----	
	3	Q	Q		1.038	1,842	1,056	.0033	431	----	----	
	4	Q	Q		1.169	1,891	1,158	.0028	408	----	----	
	5	Q	Q		1.300	2,046	1,256	.0026	388	----	----	
	6	Q	Q		1.312	2,200	1,261	.0028	385	----	----	
	7	Q	Q		1.162	2,229	1,150	.0034	408	----	----	
	8	D	D		1.181	2,782	1,150	.0042	395	----	----	
		F	N	220	1.188	2,991	1,148	.0045	389	21.9	----	0.456
		N	F	220	1.193	3,020	1,152	.0045	388	----	22.2	.454
3	9	F	N	156	.970	1,293	1,009	.0025	451	40.3	----	.368
		X	Q		1.056	1,479	1,079	.0025	435	----	----	
	10	X	F	183	1.158	2,086	1,150	.0032	410	----	31.2	.378
2	11	N	D		.827	1,388	872	.0036	463	----	----	
		N	F	158	.828	1,400	872	.0037	462	----	27.3	.431
		Q	X		.840	1,608	880	.0042	456	----	----	
	12	D	X		.852	1,668	892	.0042	457	----	----	
		F	X	167	.850	1,680	891	.0042	457	23.9	----	.446
4	13	Q	Q		.977	1,247	1,030	.0024	462	----	----	
	14	D	N		.882	1,440	936	.0033	468	----	----	
		F	N	170	.884	1,462	937	.0033	467	32.6	----	.432
		X	Q		.885	1,515	938	.0034	467	----	----	
	15	X	D		1.077	2,408	1,091	.0040	427	----	----	
		X	F	220	1.090	2,521	1,097	.0042	422	----	25.3	.477

[a]Panel behavior code: N, no flutter or data not applicable to this panel; D, low damping; F, flutter; Q, maximum q, no flutter; X, panel destroyed or not installed.

[redacted]

Airfoil ordinates, percent chord		
Station	Root ordinate	Tip ordinate
Leading edge	0.00	0.00
0.10	.27	.35
.25	.41	.54
.50	.53	.73
.75	.58	.85
1.25	.65	.97
2.50	.79	1.05
5.00	1.04	1.20
7.50	1.27	1.35
10.00	1.46	1.50
15.00	1.77	1.77
20.00	2.00	2.00
25.00	2.18	2.18
30.00	2.32	2.32
35.00	2.42	2.42
40.00	2.48	2.48
45.00	2.50	2.50
50.00	2.49	2.49
55.00	2.44	2.44
60.00	2.35	2.35
65.00	2 18	2.18
67.00	2..9	2.08
Trailing edge	.50	.50

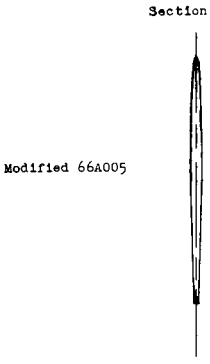

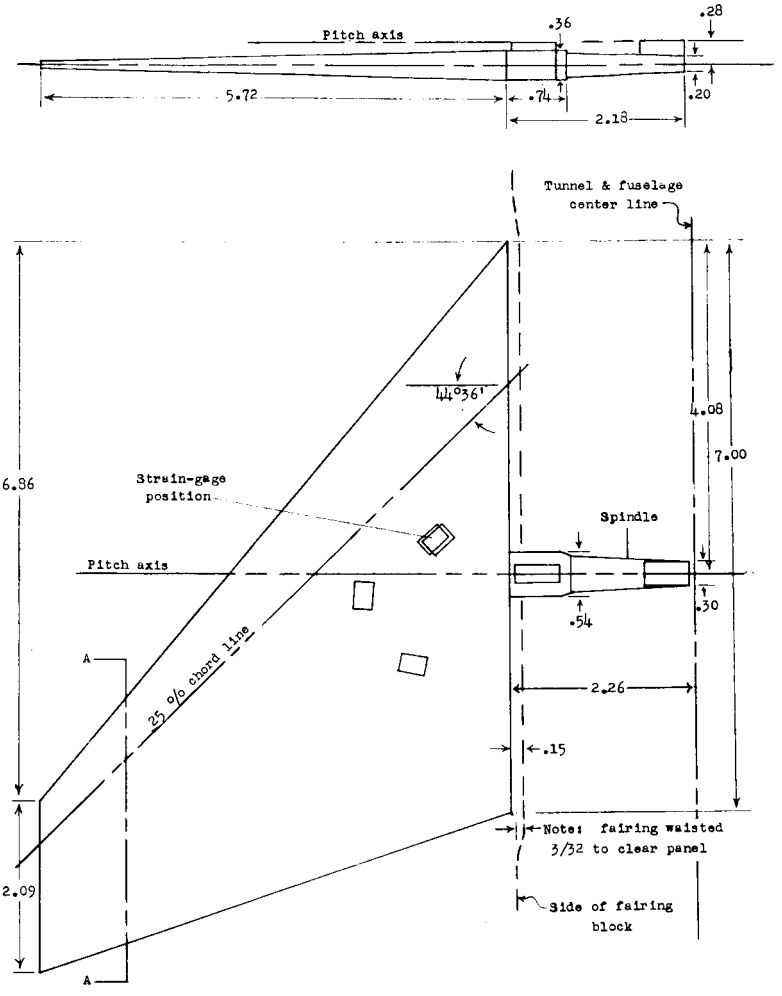

Figure 1.- Sketch of panel. Dimensions are in inches.

[redacted]

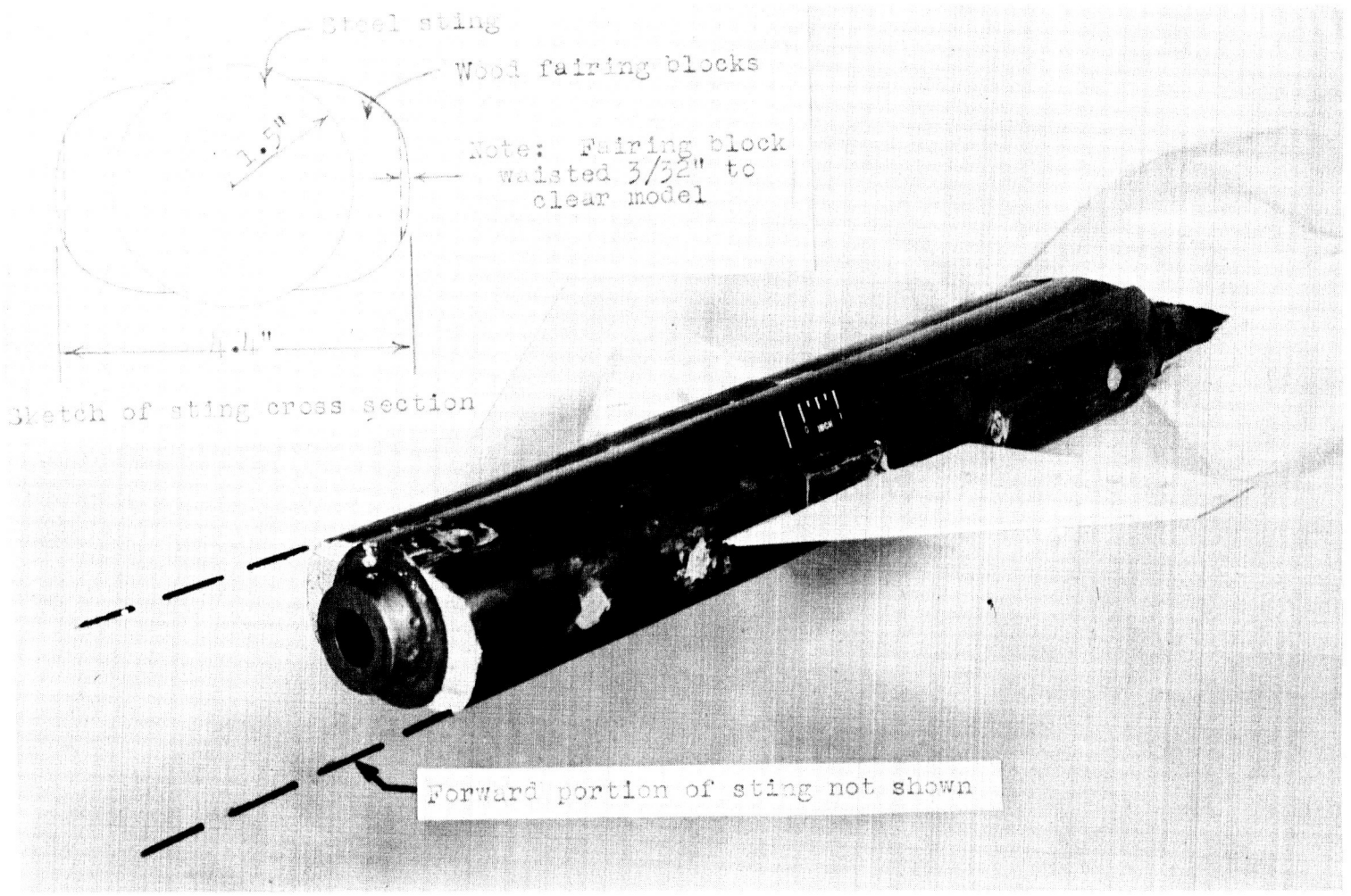

L-59-4393.1

Figure 2.- Photograph of model mounted in the sting, and sketch of sting cross section.

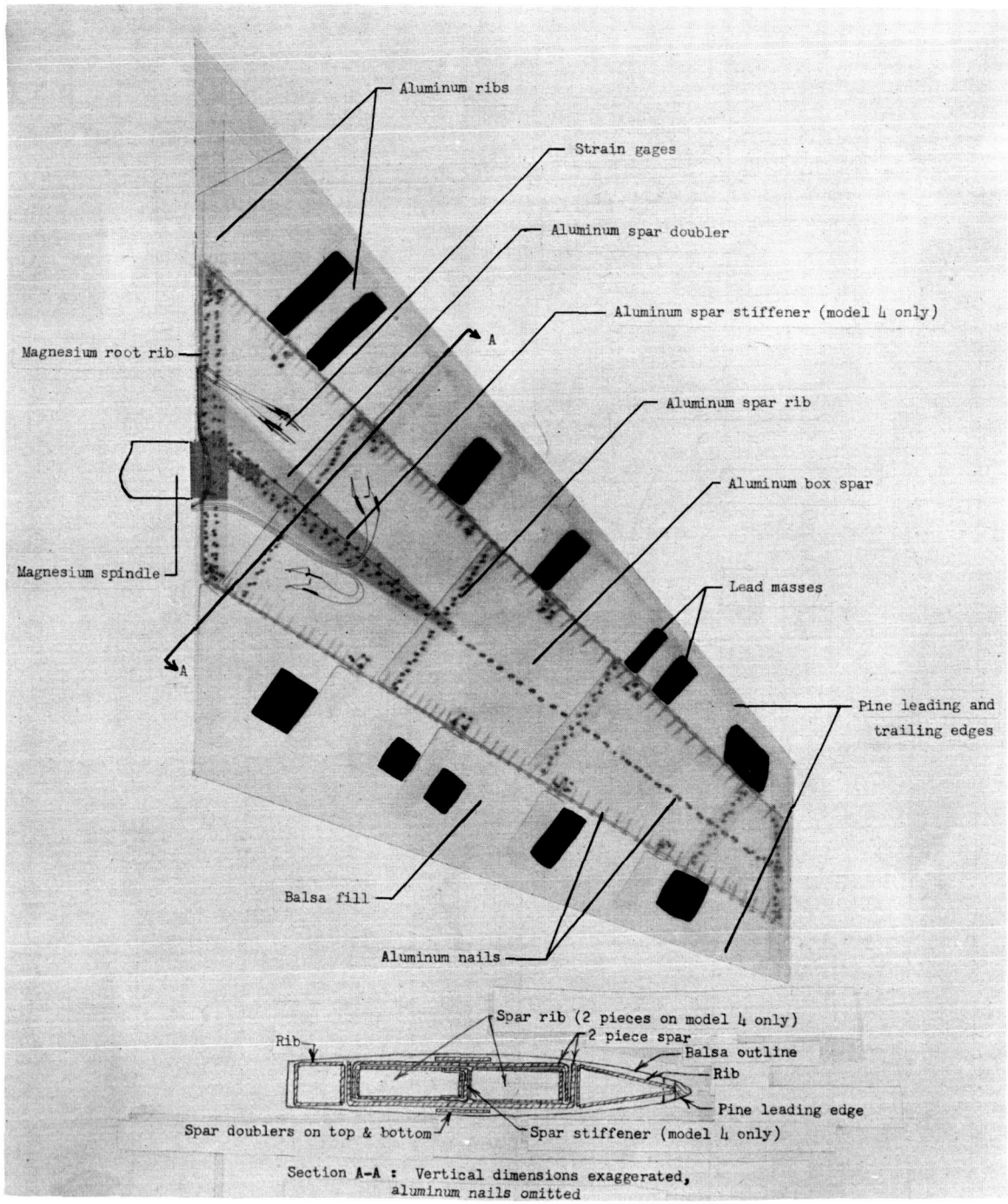

Figure 3.- X-ray photograph of panel 4R. L-60-6907

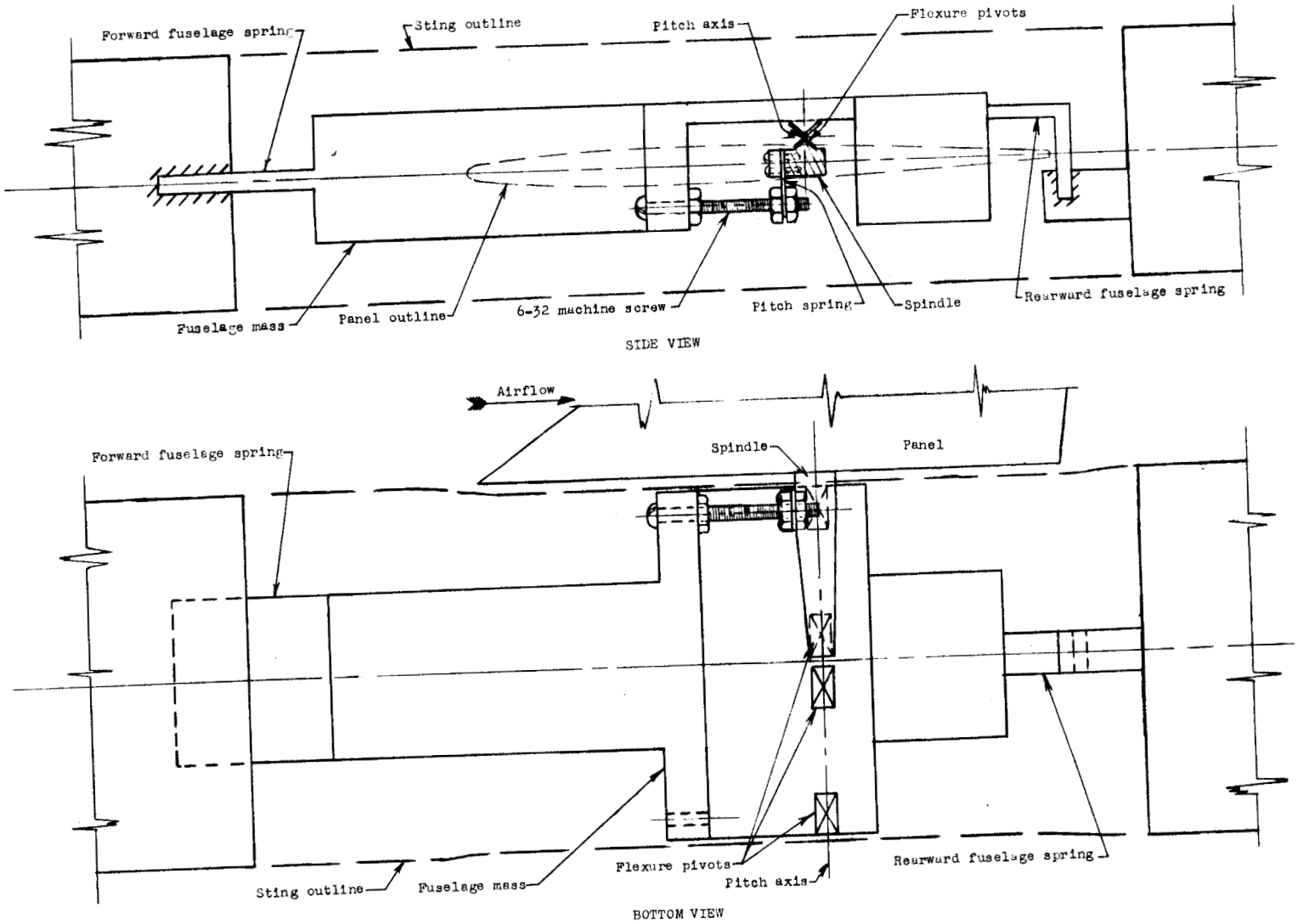

Figure 4.- Schematic sketch of panel mounting in sting fuselage.

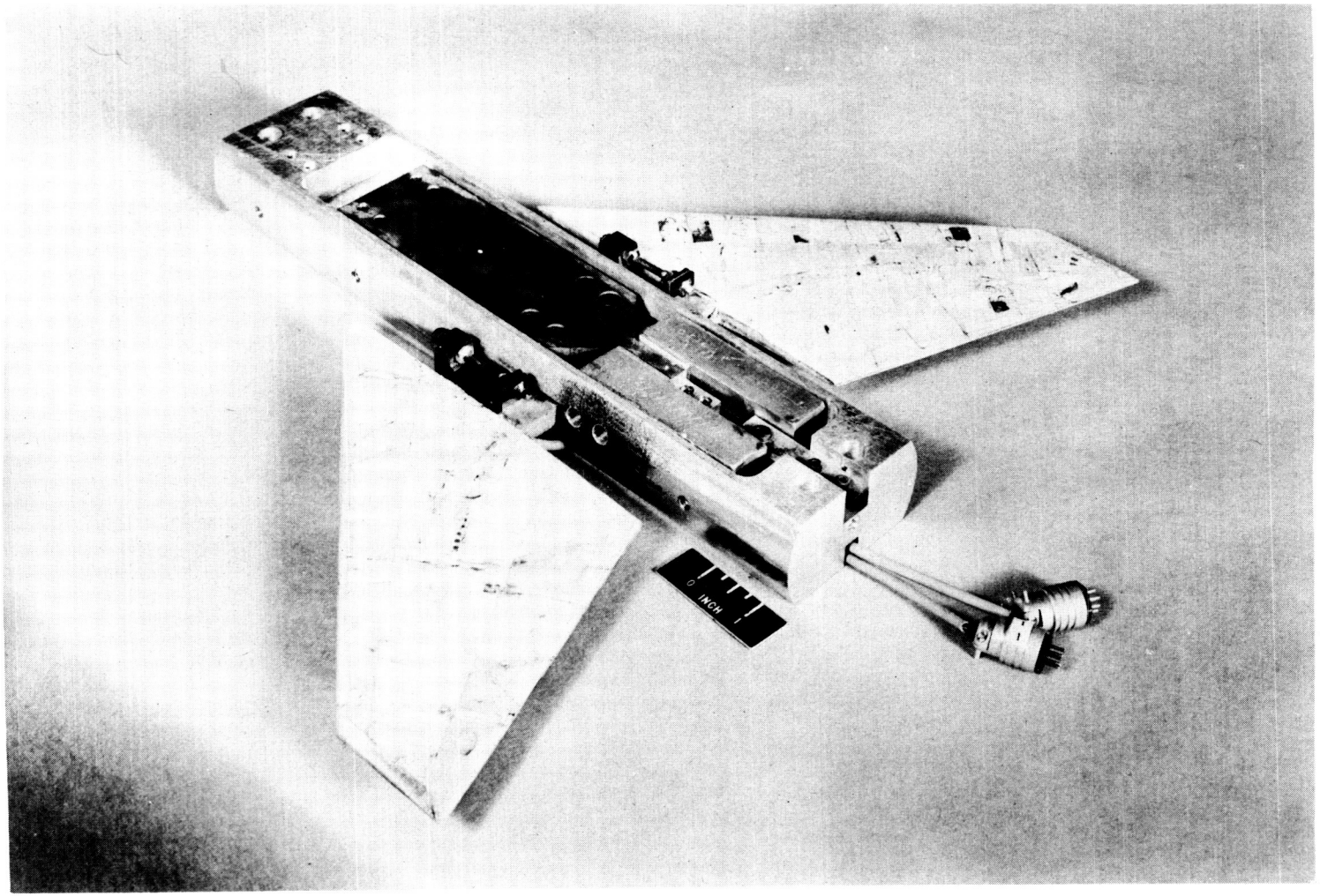

L-59-4396

Figure 5.- Photograph of model in sting mounting block, removed from sting and wooden fairing blocks.

Left panel

Mode	Frequency (cps)
f_1	112
f_2	150
f_5	297
f_8	332
f_{11}	387
f_{12}	440
No node line f_{15}	523

Right panel

Mode	Frequency (cps)
f_1	110
f_2	150
f_5	297
f_8	327
f_{11}	387
f_{12}	440

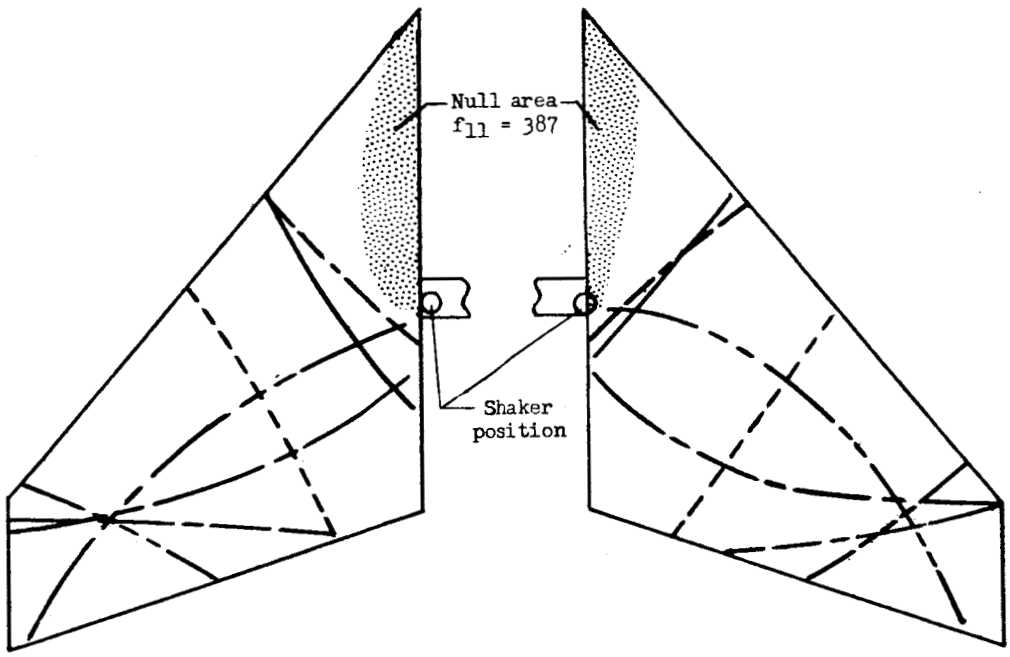

(a) Model 1.

Figure 6.- Measured natural vibration frequencies and node lines.

[redacted]

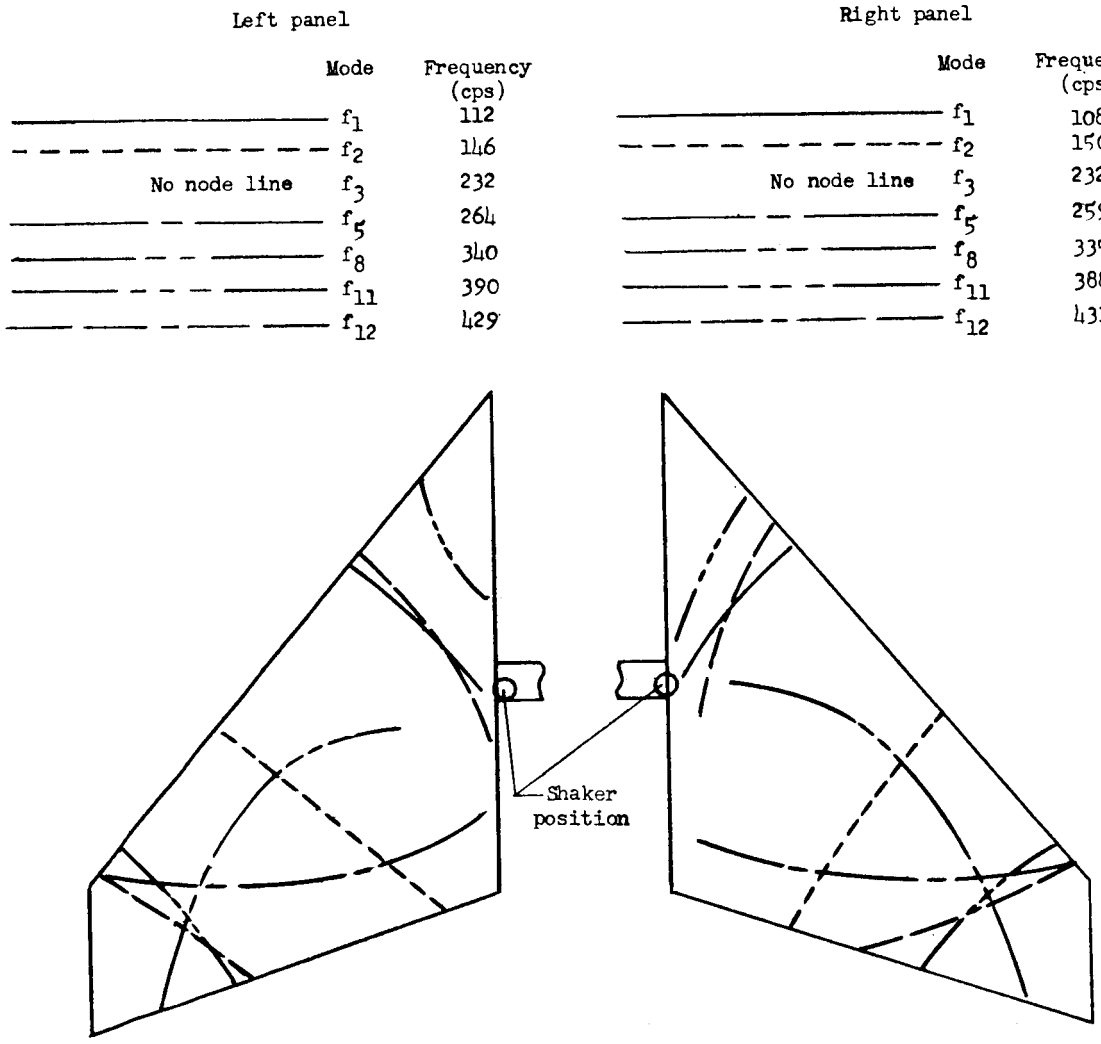

(b) Model 2.

Figure 6.- Continued.

Left panel			Right panel		
	Mode	Frequency (cps)		Mode	Frequency (cps)
———	f_1	106	———	f_1	102
- - -	f_2	145	- - -	f_2	140
No node line	f_3	182	No node line	f_3	182
No node line	f_4	237	No node line	f_4	237
——— – ———	f_5	276	——— – ———	f_5	276
——— – – ———	f_8	301	——— – – ———	f_6	283
——— ——— – ———	f_{11}	383	——— – – ———	f_8	302
——— ——— – ———	f_{12}	430	——— ——— – ———	f_{11}	383
——— ——— – – ———	f_{13}	331	——— ——— – ———	f_{12}	430
			——— ——— – – ———	f_{13}	331

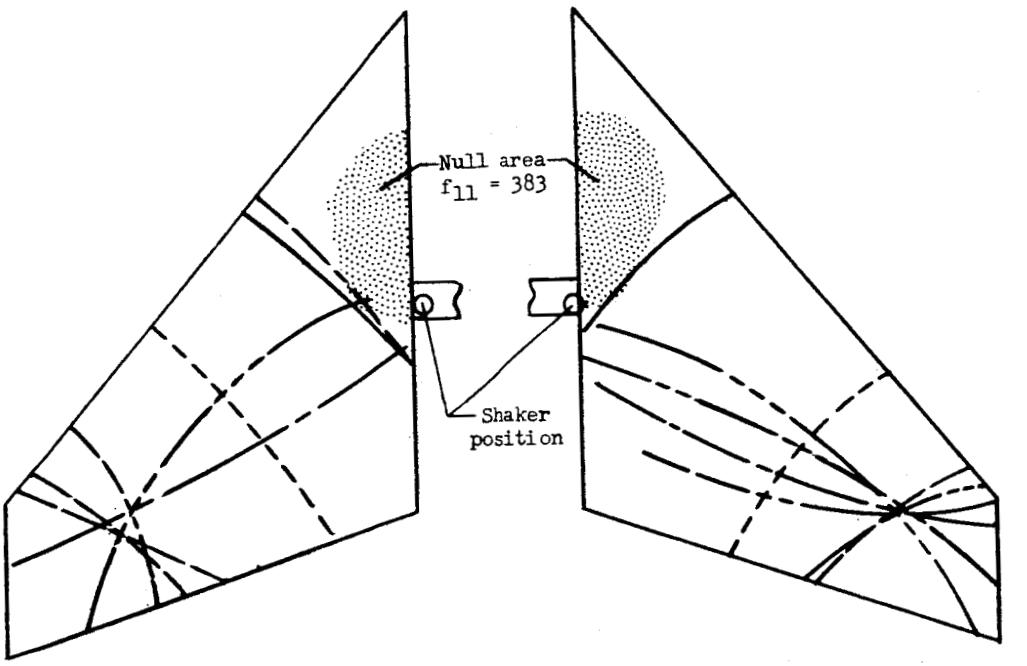

(c) Model 3.

Figure 6.- Continued.

Left panel		
	Mode	Frequency (cps)
———	f_1	108
- - - -	f_2	149
No node line	f_3	179
No node line	f_4	234-240
——— — ———	f_5	278
——— - - ———	f_7	234
——— - - - ———	f_8	300
—— —— - —— ——	f_9	264
—— —— - - —— ——	f_{11}	383
—— —— - - - —— ——	f_{12}	333
No node line	f_{14}	480
No node line	f_{15}	520
No node line	f_{16}	840

Right panel		
	Mode	Frequency (cps)
———	f_1	106
- - - -	f_2	148
No node line	f_3	179
No node line	f_4	234-240
——— — ———	f_5	278
——— - - ———	f_7	234
——— - - - ———	f_8	300
—— —— - —— ——	f_9	264
—— —— - - —— ——	f_{11}	380
—— —— - - - —— ——	f_{12}	333
No node line	f_{14}	480
No node line	f_{15}	527

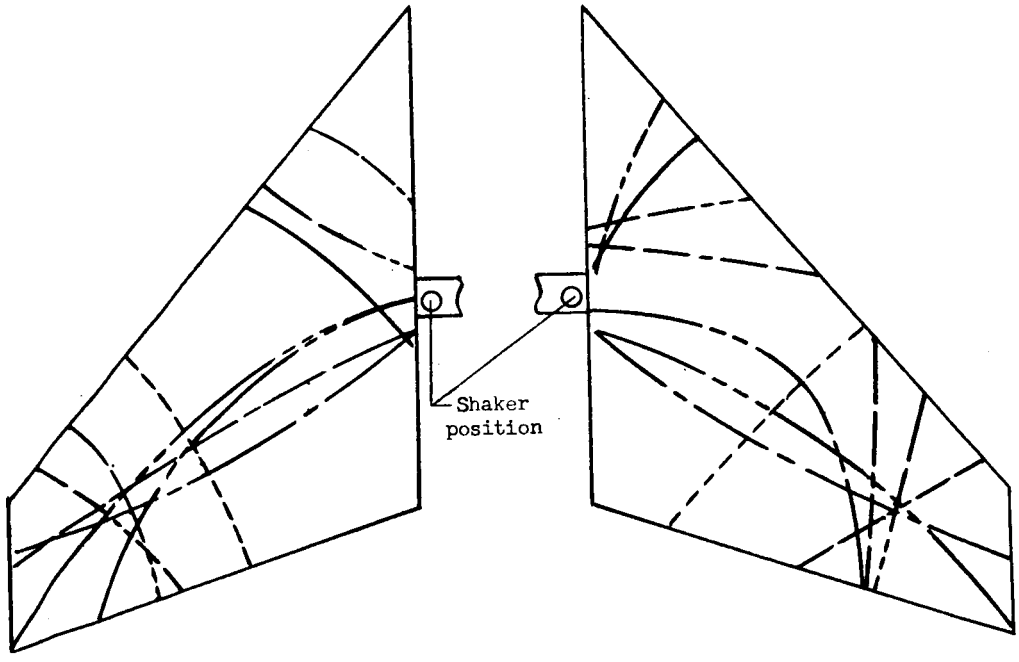

(d) Model 4.

Figure 6.- Continued.

	Mode	Frequency (cps)
———	f_1	106
– – –	f_8	300
——— — ———	f_{10}	216
——— – – ———	f_{11}	376
——— – – – ———	f_{15}	505
No node line	f_{16}	765

L-1016

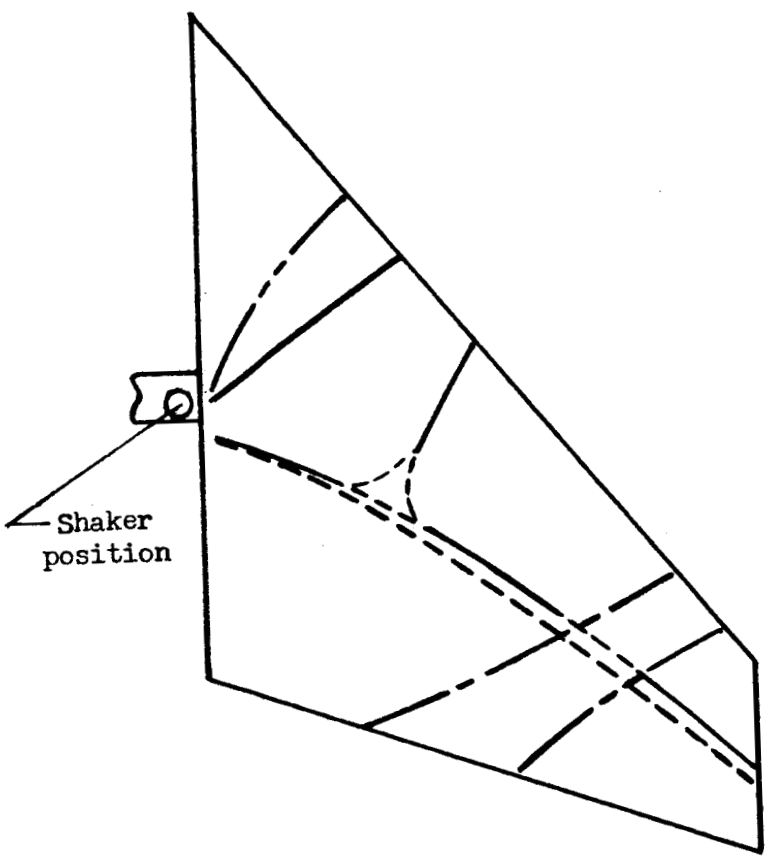

(e) Model 4, right panel alone.

Figure 6.- Continued.

[redacted]

	Mode	Frequency (cps)
———	f_1	115
No node line	f_2	143
— — — —	f_8	305
—•— - —	f_{11}	408
——- - —	f_{15}	559

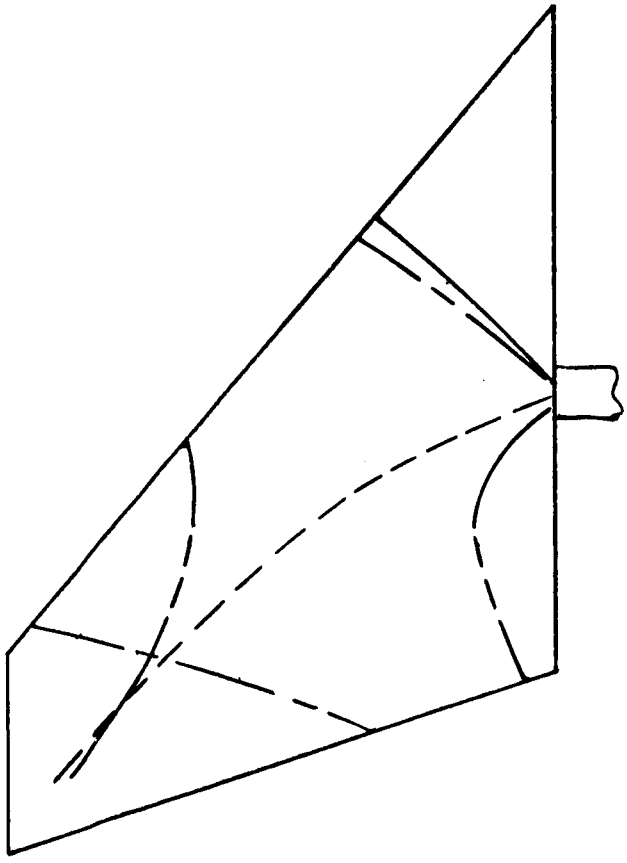

(f) Airplane scaled values.

Figure 6.- Concluded.

[redacted]

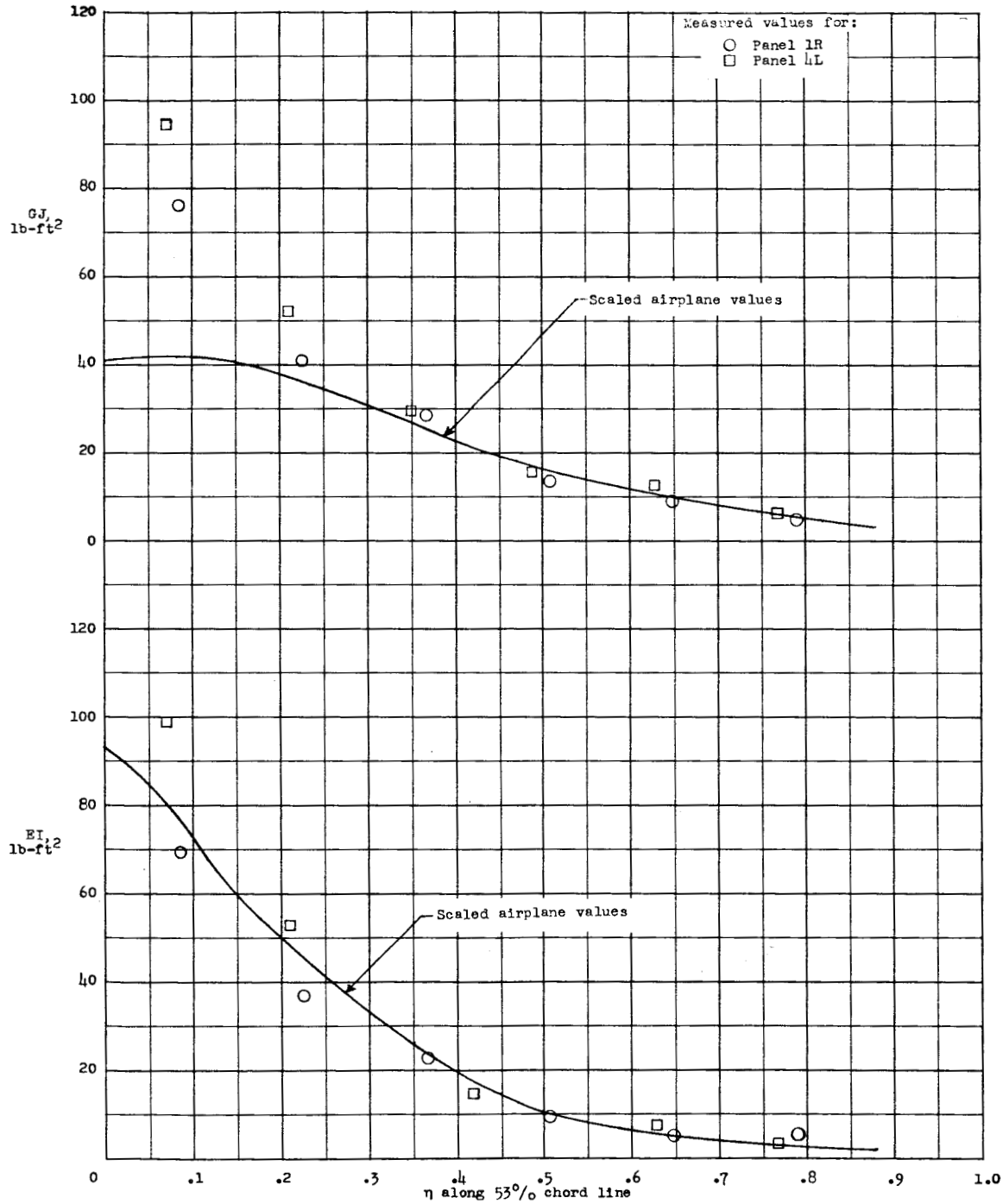

Figure 7.- Measured panel torsional and bending stiffness distributions compared with scaled airplane stiffness distributions.

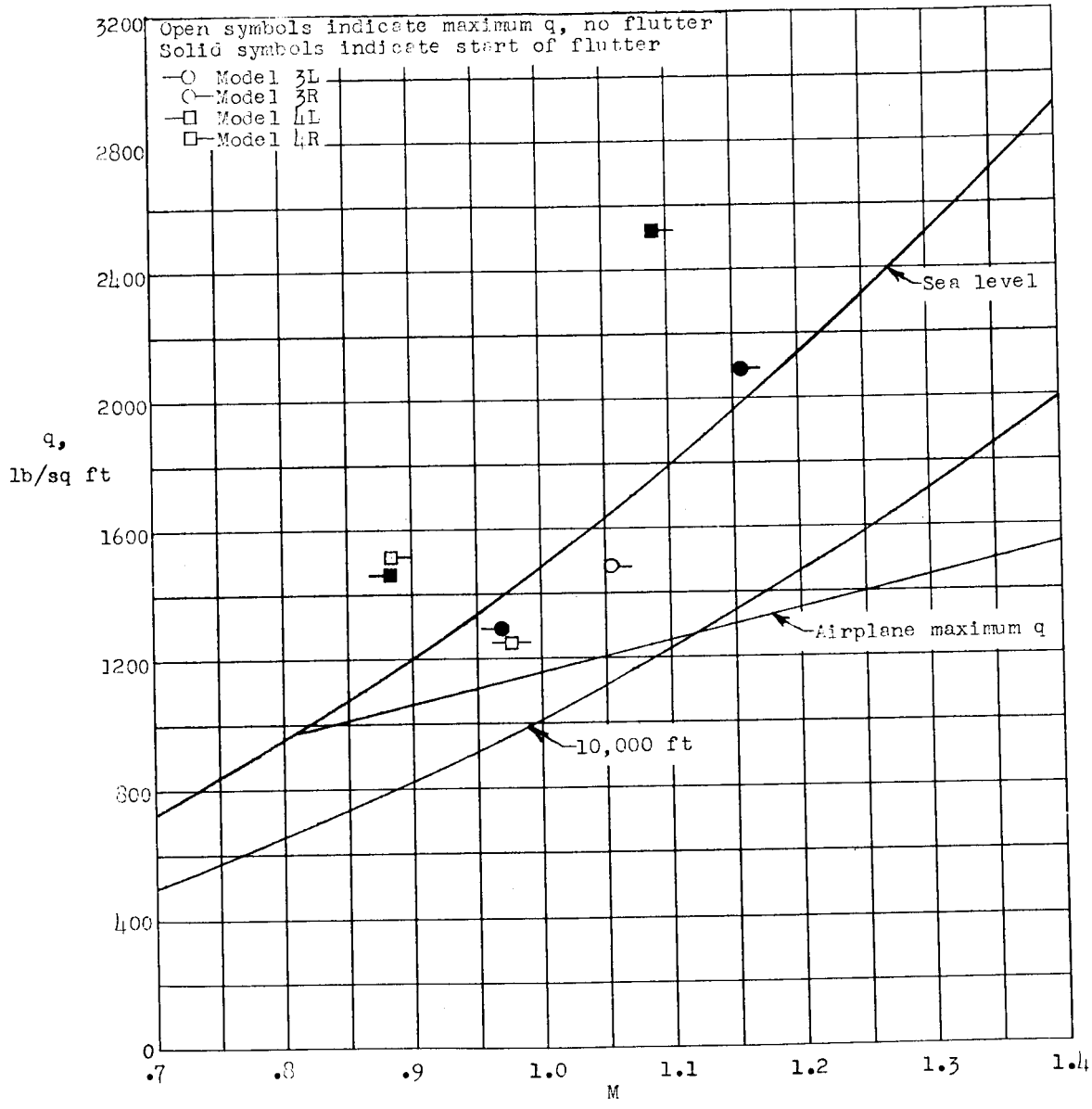

Figure 8.- Test dynamic pressure versus Mach number for models 3 and 4. k_θ is close to scaled value.

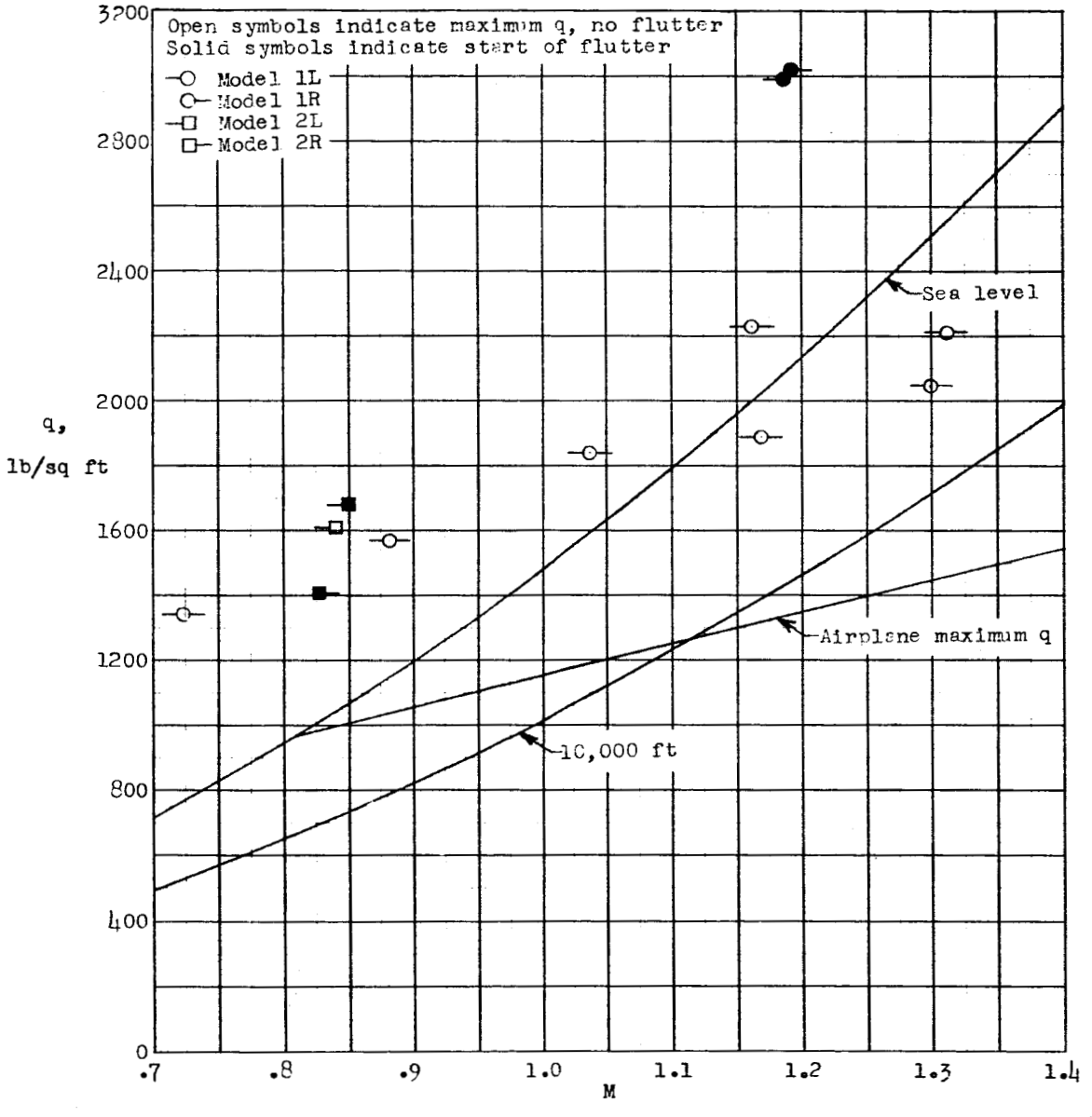

Figure 9.- Test dynamic pressure versus Mach number for models 1 and 2. k_θ averages 157 percent of scaled value.

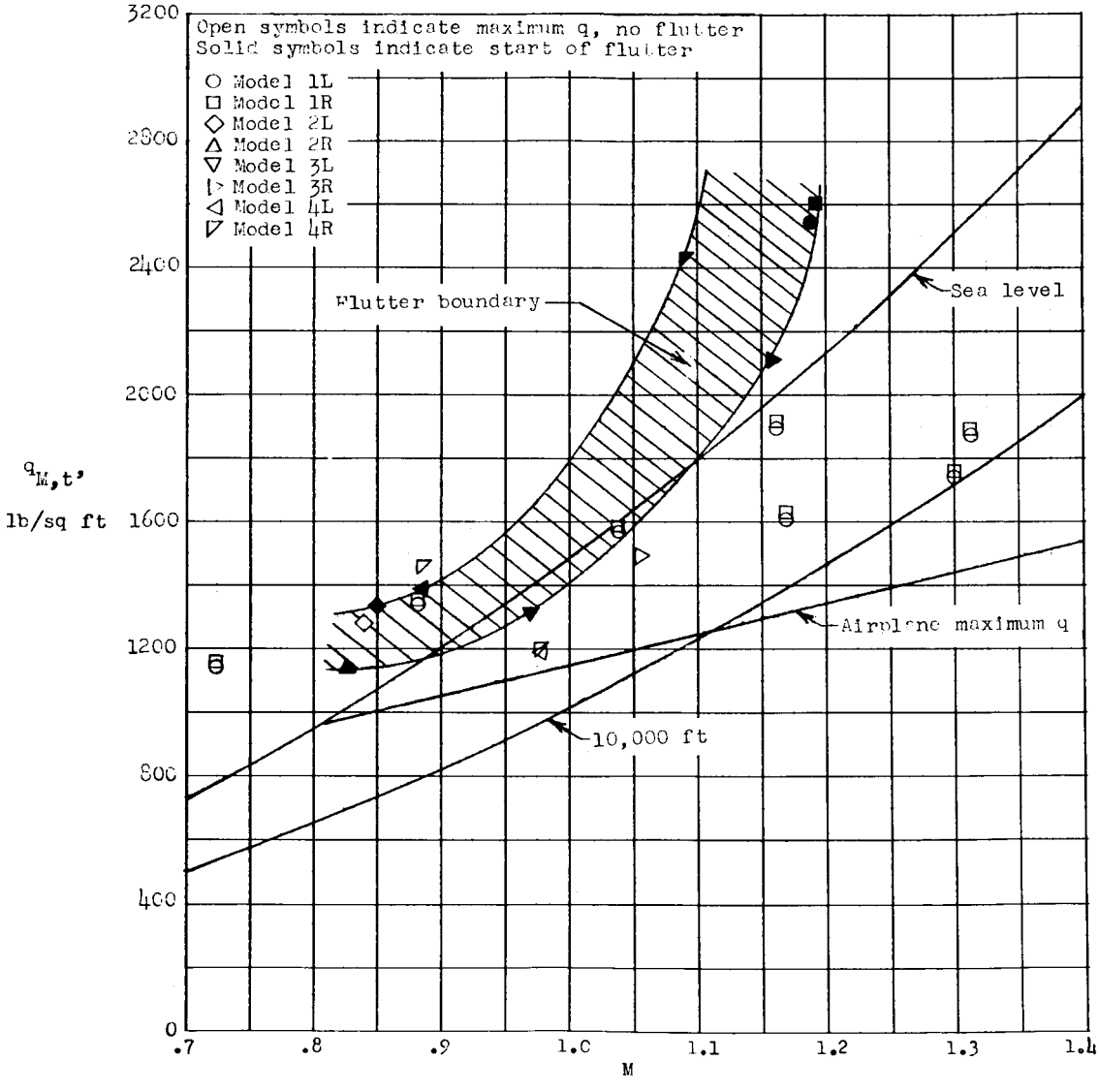

Figure 10.- Dynamic pressure versus Mach number.

L-1016